
Article:
Kunz, A, Müller, R, Homonnai, V et al. (2013) Extending water vapor trend observations over Boulder into the tropopause region: Trend uncertainties and resulting radiative forcing. Journal of Geophysical Research D: Atmospheres, 118 (11). 11,269 - 11,284 (16). ISSN: 0148-0227

https://doi.org/10.1002/jgrd.50831

Extending water vapor trend observations over Boulder into the tropopause region: Trend uncertainties and resulting radiative forcing

A. Kunz,[1,2] R. Müller,[1] V. Homonnai,[3] I. M. Jánosi,[3] D. Hurst,[4,5] A. Rap,[6] P. M. Forster,[6] F. Rohrer,[7] N. Spelten,[1] and M. Riese[1]

Received 5 April 2013; revised 10 September 2013; accepted 10 September 2013.

[1] Thirty years of balloon-borne measurements over Boulder (40°N, 105°W) are used to investigate the water vapor trend in the tropopause region. This analysis extends previously published trends, usually focusing on altitudes greater than 16 km, to lower altitudes. Two new concepts are applied: (1) Trends are presented in a thermal tropopause (TP) relative coordinate system from –2 km below to 10 km above the TP, and (2) sonde profiles are selected according to TP height. Tropical (TP_z > 14 km), extratropical (TP_z < 12 km), and transitional air mass types (12 km < TP_z < 14 km) reveal three different water vapor reservoirs. The analysis based on these concepts reduces the dynamically induced water vapor variability at the TP and principally favors refined water vapor trend studies in the upper troposphere and lower stratosphere. Nonetheless, this study shows how uncertain trends are at altitudes –2 to +4 km around the TP. This uncertainty in turn has an influence on the uncertainty and interpretation of water vapor radiative effects at the TP, which are locally estimated for the 30 year period to be of uncertain sign. The much discussed decrease in water vapor at the beginning of 2001 is not detectable between –2 and 2 km around the TP. On lower stratospheric isentropes, the water vapor change at the beginning of 2001 is more intense for extratropical than for tropical air mass types. This suggests a possible link with changing dynamics above the jet stream such as changes in the shallow branch of the Brewer-Dobson circulation.

Citation: Kunz, A., R. Müller, V. Homonnai, I. M. Jánosi, D. Hurst, A. Rap, P. M. Forster, F. Rohrer, N. Spelten, and M. Riese (2013), Extending water vapor trend observations over Boulder into the tropopause region: Trend uncertainties and resulting radiative forcing, *J. Geophys. Res. Atmos.*, *118*, doi:10.1002/jgrd.50831.

1. Introduction

[2] The upper troposphere and lower stratosphere (UTLS) is a region of strong interaction between dynamics, chemistry, and radiation. Cross-tropopause exchange processes affect the distribution of climate-relevant trace gases in the UTLS and the radiative balance at the tropopause. In addition, a change in the atmospheric trace gas composition in the UTLS, in particular, in O_3 and H_2O, has the potential to significantly affect surface climate [*Forster and Shine*, 1997; *Solomon et al.*, 2010; *Riese et al.*, 2012]. Nevertheless, in the UTLS, dynamical variability makes it difficult to accurately detect and quantify a change in trace gas distributions, in particular, water vapor, around the tropopause.

[3] The trace gas distribution in the tropopause region is influenced by a range of atmospheric processes such as the seasonal cycle in tropopause height [*Holton et al.*, 1995]. The sharp PV gradient across the tropopause acts as a transport barrier and consequently has an impact on the distribution of trace gases at the tropopause [*Kunz et al.*, 2011a, 2011b]. Trace gases such as ozone and water vapor near the tropopause are influenced in particular by transport processes, e.g., by convection in the troposphere, quasi-horizontal exchange and mixing across the jet streams, or two-way exchange processes such as stratospheric and tropospheric intrusions.

[4] All these processes may affect changes in structure and chemical composition, in particular, ozone and water

[1]Institut für Energie– und Klimaforschung: Stratosphäre, Forschungszentrum Jülich, Jülich, Germany.
[2]Now at Institute for Atmospheric and Climate Science, ETH Zürich, Zurich, Switzerland.
[3]Department of Physics of Complex Systems, Eötvös Loránd University, Budapest, Hungary.
[4]Cooperative Institute for Research in Environmental Sciences, University of Colorado, Boulder, Colorado, USA.
[5]Global Monitoring Division, NOAA Earth System Research Laboratory, Boulder, Colorado, USA.
[6]School of Earth and Environment, University of Leeds, Leeds, UK.
[7]Institut für Energie– und Klimaforschung: Troposphäre, Forschungszentrum Jülich, Jülich, Germany.

Corresponding author: A. Kunz, Institute for Atmospheric and Climate Science, ETH Zürich, CHN M 14, Universitätstrasse 16, CH-8092 Zurich, Switzerland. (anne.kunz@env.ethz.ch)

2169-897X/13/10.1002/jgrd.50831

vapor, near the tropopause, which in turn result in changed radiative effects in the atmosphere [e.g., *Kunz et al.*, 2009; *Riese et al.*, 2012]. *Kunz et al.* [2009] showed that an increase in water vapor content caused by advective and mixing-induced transport processes at the tropopause is connected with a decrease in local temperature. A trend in temperature and climate relevant trace gases such as water vapor near the tropopause may therefore be an indicator for a trend in the frequency and strength of tropopause dynamics influencing the local chemical composition. However, the highly variable character of the tropopause height and water vapor on different time scales in the UTLS makes it difficult to detect statistically significant trends of water vapor close to the tropopause.

[5] The tropopause region, i.e., the altitude region where surface climate is most sensitive to water vapor changes [*Solomon et al.*, 2010; *Riese et al.*, 2012], has usually been excluded from trend analyses of water vapor to avoid the strong variability due to tropopause dynamics. Analyses rather focused on altitudes above 16 km in the lower stratosphere [e.g., *Oltmans et al.*, 2000; *Rosenlof et al.*, 2001; *Scherer et al.*, 2008; *Hurst et al.*, 2011]. Based on the Boulder sonde data from 1980 to 2000, *Oltmans et al.* [2000] reported significant increases in stratospheric water vapor throughout the year in the altitude range 16 to 28 km, whereas these trends are statistically significant down to about 13 km in winter. Using several data sets based on different water vapor instruments, *Rosenlof et al.* [2001] reported a persistent trend in water vapor with a 1% per year increase in the stratosphere between 1954 and 2000. The analysis by *Rosenlof et al.* [2001] mainly focuses on the 21.5 hPa pressure level; at lower pressure levels, they filtered their data by tropopause height to avoid sampling biases in their analysis. Both *Scherer et al.* [2008] and *Hurst et al.* [2011] investigated the Boulder sonde series from 1980 up to 2007 and 2011 and found statistically significant positive water vapor trends in the stratosphere above 16 km.

[6] The observed water vapor trend in the stratosphere may be closely linked with climate change. A long-term change in the transport of air parcels from the troposphere into the stratosphere across the tropical tropopause could probably be the cause of a stratospheric water vapor trend [*Rosenlof et al.*, 2001; *Rosenlof and Reid*, 2008]. In the long term, water vapor has been generally increasing in the stratosphere at altitude levels above 16 km since 1980. Trends in stratospheric water vapor can be partly explained by an intensified oxidation of methane in the stratosphere and an increased entry of methane across the tropopause, but the underlying mechanisms are still not fully understood [e.g., *Röckmann et al.*, 2004; *Rohs et al.*, 2006]. In contrast, an analysis on shorter time periods between 5 and 10 years is characterized by positive and negative water vapor trend periods [*Hurst et al.*, 2011]. A sudden drop in stratospheric water vapor is observed in 2001 which is characterized by an increase in water vapor at the end of the 1990s and a decrease until around 2005 [*Randel et al.*, 2006; *Hurst et al.*, 2011]. The sudden drop in stratospheric water vapor in 2001 may be attributed to anomalously low temperatures at the tropical cold point tropopause during this period [*Randel et al.*, 2006; *Rosenlof and Reid*, 2008].

[7] Statistically significant trends in water vapor, as clearly detected in the stratosphere, have not been identified around the tropopause in the UTLS [*Oltmans and Hofmann*, 1995; *Oltmans et al.*, 2000]. The reason is that investigating higher-altitude levels in the stratosphere allows an analysis without taking into account the strong variation of water vapor on a synoptic time scale, which is influenced by fluctuations of the tropopause height. Based on analyses of radiosonde data from the tropics to the poles in the period 1980–2004, the tropopause height itself has a positive trend (0.64 ± 0.21 km/decade) in the global mean and the respective tropopause temperature is globally decreasing (-1.70 ± 0.09 K/decade) [*Seidel and Randel*, 2006]. The observed tropopause height increases were closely associated with a warming in the troposphere and cooling in the stratosphere [*Sausen and Santer*, 2003]. Nevertheless, serious uncertainty recently arose about a decreasing trend in tropical tropopause temperatures due to problems with the radiosonde measurements used to construct long–term temperature records [*Wang et al.*, 2012]. According to *Wang et al.* [2012], the uncertainty of trends of tropopause temperatures and heights based on radiosonde measurements seems to be greater than previously expected.

[8] Here trends of water vapor in the UTLS region are estimated by taking into account the dynamically driven variability in this region. This study makes use of water vapor data based on the longest record of balloon-borne measurements over Boulder, Colorado, for 30 years (1981–2011). Hitherto, this data set has only been analyzed for trends using averaging in geopotential height coordinates relative to the sea level. Here the trend analyses of these data will be extended into the tropopause region using geopotential height coordinates relative to the tropopause height. To preserve features of the tropopause that are variable in time, the temperature and water vapor fields are analyzed relative to the tropopause level following the commonly used method [e.g., *Birner et al.*, 2002; *Kunz et al.*, 2009]. Furthermore, the Boulder sonde station (40°N) is in a region where measurements are strongly influenced by the dynamics and seasonality of the subtropical jet stream. The dependence on the location of the subtropical jet stream will therefore be taken into account when discussing the following questions: (1) How accurately can we quantify the variability and trends in UTLS water vapor observed over Boulder? (2) What is the impact of water vapor change over Boulder on radiative forcing of the atmosphere?

[9] The paper is structured as follows. In section 2 the observations used to calculate the trends in the tropopause region are introduced, and the analysis technique for this study is presented. The results are presented in section 3, and a discussion and conclusion is given in section 4.

2. Data and Methodology

2.1. Boulder Sonde Data

[10] The modern 30 year record of water vapor measurements over Boulder, Colorado (40°N, 105°W), which started in 1980, is used to study trends in the tropopause region. In this analysis the data record from 1981 to 2011 based on 333 balloon flights is used. Usually, one to three flights are performed per season with exceptional seasons of up to seven flights within the last 10 years.

[11] Water vapor is measured every 5–10 m (1–2 s) between the surface and the middle stratosphere ($\approx$ 28 km)

by the NOAA frost point hygrometer (FPH). For a better usage in models and papers, especially those examining temporal trends, mean water vapor mixing ratios are computed in 250 m vertical bins and provided for scientific usage.

[12] The original design of FPH instrument has improved throughout the years [e.g., *Vömel et al.*, 1995; *Oltmans et al.*, 2000], but the fundamental calibration procedure remained the same [*Hurst et al.*, 2011]. The NOAA FPH is based on a chilled mirror principle. A thin, stable layer of frost on a temperature-controlled mirror is measured as air flows through the hygrometer. Changes in frost coverage detected by the photo diode are countered by rapidly adjusting the amount of mirror heating against persistent cryogenic cooling. A stable frost layer implies equilibrium between the ice and the ambient water vapor. Under these equilibrium conditions, the ice surface temperature (frost point temperature) is directly related to the partial pressure of water vapor in the air stream around the mirror. The water vapor mixing ratio and relative humidity can be calculated from the frost point temperature using the Clausius-Clapeyron equation and simultaneous measurements of ambient pressure and temperature by a radiosonde. See *Hurst et al.* [2011] for a more detailed measurement description.

[13] NOAA FPH measurements of water vapor in the stratosphere are made with a precision and estimated accuracy of better than 4% and 10%, respectively [*Vömel et al.*, 1995; *Hurst et al.*, 2011]. The water vapor detection range is from 0.5 to 25,000 ppmv and the frost point temperature uncertainty is 0.5°C between –95°C and 25°C.

2.2. Halogen Occultation Experiment (HALOE) Satellite Data

[14] Water vapor data from the Halogen Occultation Experiment (HALOE) on board the Upper Atmosphere Research Satellite for the period from 1991 to 2005 are included in this analysis. The systematic and random uncertainty of single water vapor profiles in the lower stratosphere is between 14 and 24%, whereas the agreement with correlative measurements is typically better than 10% [see *Grooß and Russell III*, 2005, and references therein]. The total available HALOE water vapor data are presented here for all longitudes within the ±5° latitude band around 40°N. HALOE water vapor data show realistic climatological structures from 200 to 0.1 hPa, with increasing mixing ratio with increasing altitude throughout the stratosphere and a strong dehydration in the Antarctic vortex in winter and spring [*Grooß and Russell III*, 2005]. HALOE data have also been used in combination with Boulder sonde statistics for the evaluation of water vapor trends and variability in the lower stratosphere [e.g., *Scherer et al.*, 2008; *Solomon et al.*, 2010]. The 2–3 km vertical resolution of HALOE water vapor retrievals in the UTLS provides a compelling reason to average the Boulder FPH data in 2 km altitude bins for the purpose of trend analysis.

2.3. Radiation Code

[15] To estimate the radiative effects of water vapor changes in the tropopause region over Boulder the off-line version of the *Edwards and Slingo* [1996] radiative transfer code is used with six bands in the shortwave, nine bands in the longwave, and a delta-Eddington two-stream scattering solver at all wavelengths. A single column configuration was considered with 119 vertical levels representing an altitude range of 1.2 to 30.7 km (816.58 to 11.85 hPa pressure level range). The model used mean 2003–2011 temperature and ozone profiles from the Boulder sonde observations. Section 3.4 presents results of four experiments which were simulated based on different water vapor profiles: (i) a reference experiment using the 1981 profile, (ii) a mean trend experiment using the 30 year mean trend, (iii) an upper limit experiment using the 30 year mean trend plus 2σ trend uncertainty, (iv) a lower limit experiment using the 30 year mean trend minus 2σ trend uncertainty. Water vapor radiative forcings were then estimated by comparing each of the ii–iv experiments to the i reference experiment. Both instantaneous and stratospherically adjusted (using the fixed dynamic heating approximation) radiative forcings were calculated and are presented in section 3.4.

2.4. Tropopause-Referenced Trends

2.4.1. Calculation of the Thermal Tropopause

[16] In this analysis the thermal tropopause is calculated separately for each of the Boulder sonde profiles. Here the thermal tropopause is based on the vertical temperature lapse rate with geopotential height. According to the *World Meteorological Organization* [1957], the first tropopause is defined as the lowest level at which the lapse rate is 2 K/km or less. The average lapse rate between this level and all higher levels within 2 km may not exceed 2 K/km. If above the first tropopause level, the average lapse rate between any level and all higher levels within 1 km exceeds 3 K/km, a second tropopause is defined by the same criterion as for the first tropopause. The first tropopause, 1.TP, will be referred to as "thermal tropopause" and the second tropopause, 2.TP, as "double tropopause" in the following.

[17] To preserve features of the tropopause that are variable in time, the relevant variables, e.g., water vapor and temperature, are first interpolated on 0.25 km equidistant vertical levels relative to the thermal tropopause. This is done for each sonde profile separately. Then, further parameters such as the buoyancy frequency squared, N^2, may be calculated using geopotential heights in this tropopause relative coordinate system. In the following, we consider two different coordinate systems. First, the original geopotential heights with the sea level as the point of origin are referred to as "sea level relative coordinates." Second, a coordinate transformation of geopotential heights using the tropopause as the point of origin yields "tropopause relative coordinates."

2.4.2. Mean Vertical Profiles in Sea Level and Tropopause Relative Coordinates

[18] Figure 1 presents the mean vertical profiles of water vapor, temperature, and static stability in tropopause and sea level relative coordinates for the Boulder sonde data separately for JJA (June, July, August) and DJF (December, January, February) from 1981 to 2011. The altitude in this figure represents a relative altitude $z_{\mathrm{rel}} = z_{\mathrm{TP}}^{\mathrm{mean}} + (z - z_{\mathrm{TP}})$. This altitude is calculated as sum of the mean tropopause height for all available sonde data, $z_{\mathrm{TP}}^{\mathrm{mean}}$, with the distance of the measurement altitude from the tropopause height, i.e., $z - z_{\mathrm{TP}}$, for each individual profile.

[19] In DJF, the mean N^2 profile based on tropopause relative coordinates exhibits a sharp increase across the thermal tropopause and a pronounced maximum just above

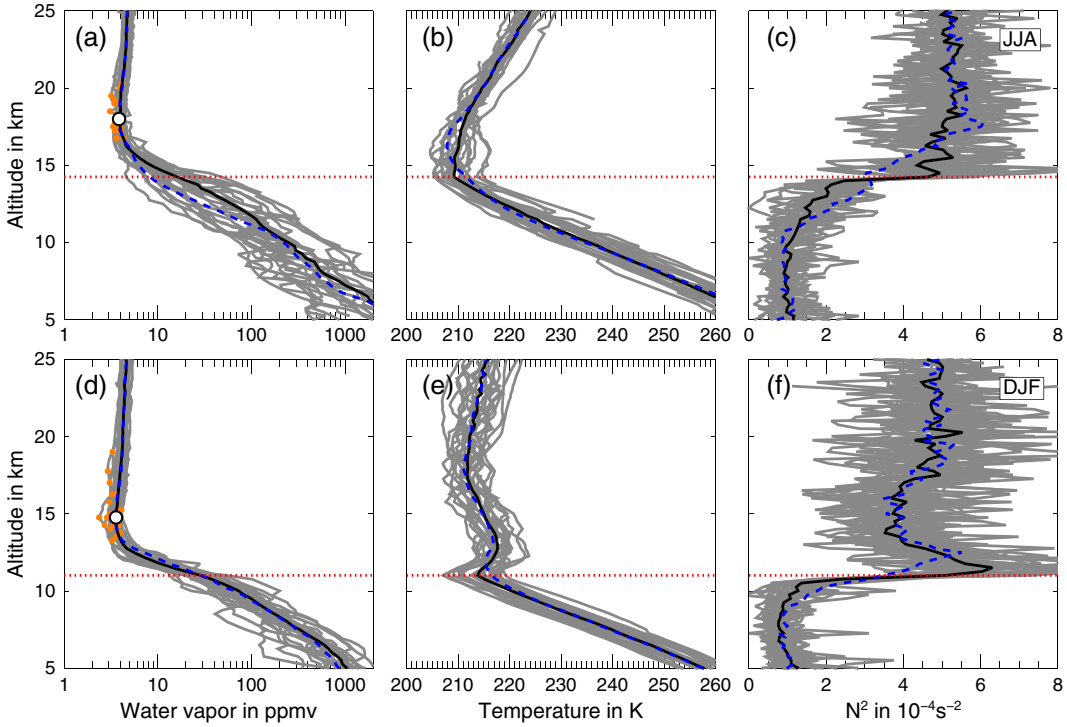

Figure 1. (a and d) Seasonal mean vertical profiles of water vapor in ppmv, (b and e) of temperature in K, and (c and f) buoyancy frequency squared N^2 in $10^{-4}s^{-2}$. Top panels show the profiles for JJA and bottom panels for DJF. Seasonal mean vertical profiles for single years from 1981–2011 (gray lines) and 30 year seasonal mean profiles (black solid lines) averaged in tropopause relative coordinates. 30 year mean profiles based on sea level relative coordinates are blue dashed. Mean tropopause height (red dotted line) is 14.25 km in JJA and 11.58 km in DJF. Orange (white) dots indicate the location of minimum water vapor for the single year (30 year) mean vertical profiles.

the tropopause in comparison to the mean profile based on sea level relative coordinates. The maximum in mean N^2 right above the thermal tropopause is smoothed out in sea level relative coordinates. Similarly, in both JJA and DJF (Figures 1b and 1e), the mean temperature profile in tropopause relative coordinates shows a much sharper gradient reversal and a lower minimum temperature at the tropopause compared to the mean profile in sea level relative coordinates.

[20] In case of water vapor, there is also a difference in mean vertical profiles when using tropopause and sea level relative coordinates. In DJF, this difference is less than 1 ppmv and is not as pronounced as in JJA, when the mean water vapor is two times higher around the tropopause ($\approx$ 10 ppmv) in tropopause than in sea level relative coordinates. By using a tropopause relative coordinate system, substantial differences in mean vertical profiles of water vapor, temperature, and buoyancy squared arise in the region around the tropopause. Depending on season these differences approximately appear between 11 and 17 km over Boulder. Above 17 km, there is no obvious difference in the seasonal mean when using tropopause or sea level relative coordinates. Therefore, results from earlier trend studies for altitudes greater than 17 km should not be influenced by the respective coordinate system used.

[21] The altitude of the minimum water vapor (see Figure 1, white dots), which is often referred to as the hygropause [e.g., *Kley et al.*, 1979, 1982], is not affected by the averaging method. By using both tropopause and sea level relative coordinates, the minimum water vapor location in the mean vertical profile is found at around 3.5 km above the mean tropopause, an altitude region where the two mean vertical water vapor profiles based on tropopause and sea level relative coordinates agree with each other. In JJA, the hygropause is at 18 km with 3.85 ppmv, and in DJF, it is at 14.78 km with 3.58 ppmv. These values are comparable with those reported by *Kley et al.* [1979] who found a minimum water vapor of 3.6 ppmv at an altitude of 2 to 3 km over the tropopause for a station at Wyoming (41°N).

[22] However, using sea level relative coordinates leads to a smoothed tropopause structure and thus influences the mean vertical profile of water vapor near the tropopause. Trends are thus estimated in a tropopause relative coordinate system in 2 km layers around the tropopause from –2 km below the tropopause up to 10 km above the tropopause level.

2.4.3. Estimation of Linear Trends and Significance

[23] Trends are calculated by simple linear regression fits of the average mixing ratios within the 2 km altitude layers relative to the tropopause for each sonde profile. These trends are determined by minimizing the chi-square error statistics. Uncertainties of the trends are reduced by the exclusion of statistical outliers before calculating the average mixing ratios within each layer. For this purpose

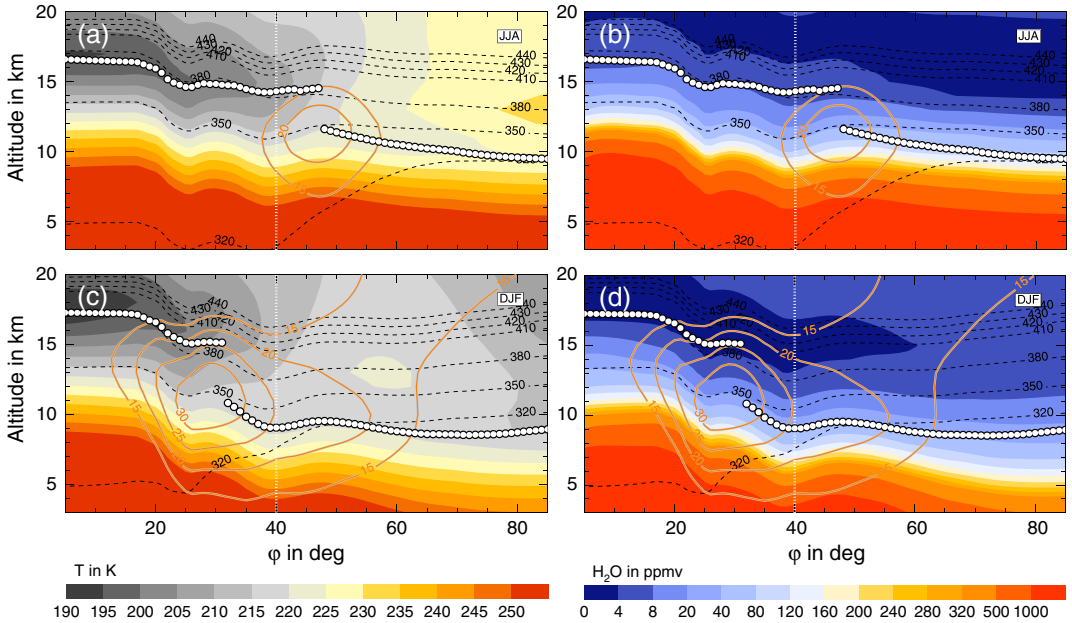

Figure 2. (a and c) Seasonal mean temperature in K and (b and d) water vapor in ppmv at the λ = 105°W longitude of the Boulder station. This climatology is based on ERA-Interim reanalysis fields from 1979 to 2012 [*Dee et al.*, 2011]. The latitude φ = 40°N of the station is marked by the vertical white dotted line. Isolines of mean zonal wind speed are colored in orange, and isolines of mean potential temperature are black dashed. The mean thermal tropopause is highlighted by white dots.

measurements are used within two standard deviations around the 30 year mean for each 2 km layer.

[24] For each of the calculated trends the significance at the 95% confidence level is determined, which will be calculated and presented for all trends reported in this paper. The significance is tested as follows: The data set, which forms the basis of a calculated trend, is shuffled to create a new artificial data set which is normally distributed around its mean. This procedure is repeated 1000 times. For each of the 1000 new artificial data sets, a linear fit regression analysis is performed as for the original data set and the corresponding trend is determined. Then, the distribution of these 1000 artificial trends is compared with the trend of the original data set. If the value of the original trend is larger than two standard deviations around the mean of the 1000 artificial trends, the original trend is tested as statistically significant at the 95% confidence level.

3. Results

3.1. ERA-Interim Water Vapor and Temperature Climatology at Boulder

[25] The Boulder sonde station is located at 40°N. Atmospheric conditions in this latitude region are strongly influenced by the seasonal cycle of the location of the subtropical jet stream as will be discussed in the following.

[26] Figure 2 shows seasonal mean cross sections of water vapor and temperature at 105°W, the geographical longitude of Boulder, in the Northern Hemisphere based on 1979–2012 ERA-Interim reanalysis fields produced by the European Centre for Medium-Range Weather Forecasts (ECMWF) [*Dee et al.*, 2011]. The core of the subtropical jet stream is located at around 30°N during DJF. When the wind speed weakens and the jet stream moves northward in JJA, the jet core is at around 45°N. Thus, Boulder lies equatorward of the jet location in JJA and poleward in DJF. The mean height of thermal tropopause at 40°N is around 15 km in JJA and around 9 km in DJF. There is a lower mean water vapor mixing ratio of 8 ppmv and a lower temperature of 205 K at the tropopause in JJA and a higher mean water vapor mixing ratio of 50 ppmv and a higher temperature of 220 K at the tropopause in DJF. The Boulder sondes therefore mostly sample high tropopauses with tropical characteristics of water vapor and temperature in JJA, whereas in DJF, the sonde profiles are largely influenced by low tropopauses with extratropical temperature and water vapor characteristics.

[27] The dynamics in the UTLS over Boulder also has an influence on the sharpness of the tropopause region. The tropopause inversion layer (TIL) at high latitudes usually has a seasonal cycle with higher maximum buoyancy frequency squared in summer than in winter [*Birner*, 2006]. In the tropics the opposite seasonal cycle is found, with higher maxima in winter than in summer [*Grise et al.*, 2010]. The buoyancy frequency squared profiles over Boulder show a greater maximum in buoyancy frequency squared in DJF than in JJA (see Figures 1c and 1f). The sonde profiles may likely sample air masses of the tropical TIL in JJA and of the extratropical TIL in DJF. The seasonal variation of the jet stream location may additionally influence the strength of the TIL over Boulder.

[28] These dynamical and chemical influences in the UTLS region over Boulder should be kept in mind when performing a trend analysis of Boulder sonde data in the following. The paper first starts with statistics and trend evaluation of the tropopause height observed by the Boulder

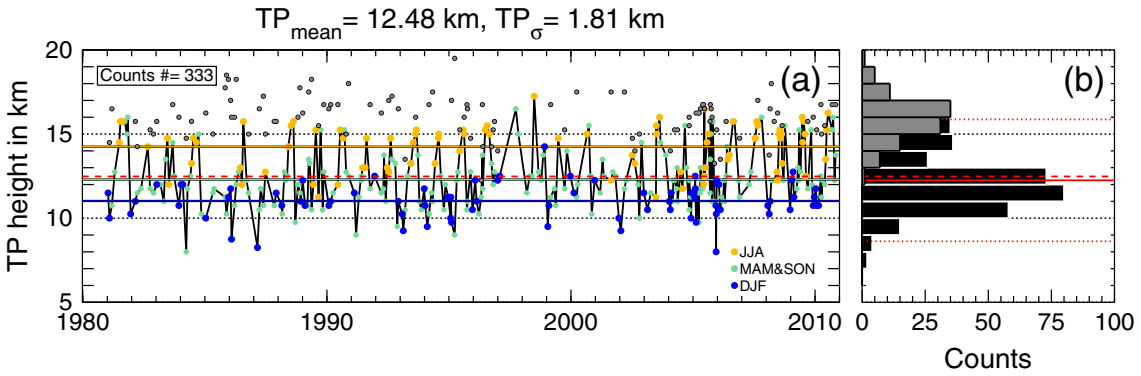

Figure 3. (a) Tropopause height over Boulder for all sonde profiles (black solid line), different seasons are indicated by colored dots. The mean tropopause height throughout the seasons (red dashed line) and for the different seasons (colored solid lines) is shown. Double tropopauses are plotted as gray dots. (b) Counts of tropopause height (black bars) and double tropopause height (gray bars). Mean tropopause (red dashed line), median tropopause (red solid line), and two standard deviations around the median (red dotted lines) are shown. Black dashed lines at 10 and 15 km are shown for orientation.

balloon sondes and proceeds with the evaluation of these observed water vapor and temperature fields in the vicinity of the tropopause.

3.2. Tropopause Over Boulder

3.2.1. Tropopause Height Characteristics

[29] Figure 3a shows the tropopause height for the 333 Boulder sonde profiles from 1981 to 2011 used in this study. There is an obvious seasonal cycle in tropopause height with an amplitude of around 5 km. The mean tropopause height for the entire time series is 12.48 km with a standard deviation of 1.81 km. A pronounced bimodal distribution of the tropopause height exists, with a first maximum at 11 km, a second maximum at around 15 km (Figure 3b). This bimodal structure in tropopause height is a well-known feature for the Northern Hemisphere subtropics, it represents the separation between the tropical and extratropical tropopause at around 14 km [*Hoinka*, 1997; *Seidel and Randel*, 2007; *Pan and Munchak*, 2011]. The second maximum of tropopause height at higher altitudes agrees well with the maximum in the distribution of double tropopause heights. Double tropopauses are found between 13 and 19 km over Boulder.

[30] A separation of the data according to sonde profiles in JJA (yellow dots), in DJF (blue dots), and MAM and SON (green dots) removes the seasonal cycle in tropopause height (Figure 3a). The second maximum in the distribution of tropopause heights at around 15 km remains in JJA, the first maximum at 11 km remains in DJF, and the two other seasons (MAM, SON) are characterized by tropopause heights in between these two maxima. During DJF most of the Boulder sonde profiles represent extratropical tropopause characteristics, and during JJA rather tropical tropopause characteristics. Consequently, when averaging the Boulder sonde data, without distinguishing between DJF and JJA data, the averages will be influenced by midlatitude and tropical tropopause characteristics.

[31] Following *Pan and Munchak* [2011], the break in the tropopause in the vicinity of the subtropical jet stream is considered here. The Boulder sonde data clearly reveal domains with different air mass types which will be addressed in the analysis of this work as follows:

[32] 1. D1: Tropical tropopause height characteristics, i.e., TP > 14 km, representative for JJA.

[33] 2. D2: Transitional (subtropical) tropopause height characteristics, i.e., 12 km < TP < 14 km, representative for MAM and SON.

[34] 3. D3: Extratropical tropopause height characteristics, i.e, TP < 12 km, representative for DJF.

[35] Before performing the trend analysis of tropopause height based on the three different tropopause domains, the frequency of these domains in the region around Boulder (40°N, 105°W) is tested. For this purpose, daily radiosonde data obtained at Denver station (39.75°N, 104.87°W) are used for the period 1979–2012. These data are freely available on the website of the University of Wyoming (http://

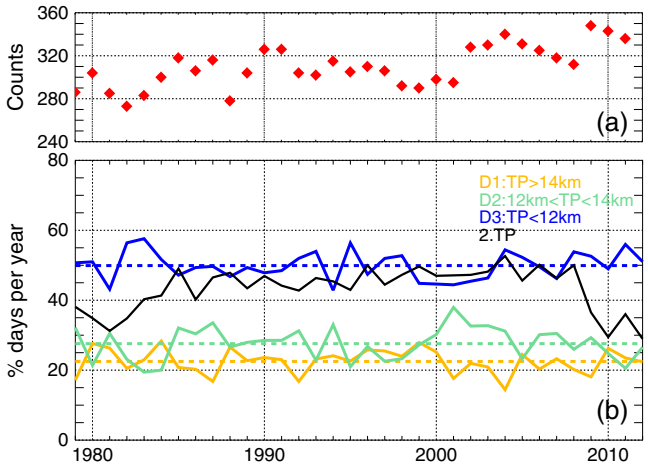

Figure 4. (a) Number of daily radiosonde profiles per year at Denver station (39.75°N, 104.78°W) from 1979 to 2012. (b) Percentage of days per year with air mass characteristics of the tropical (D1), transitional (D2), and extratropical (D3) domains (colored solid lines). Note that for the different years, these percentages are based on varying counts of profiles as shown in Figure 4a. The mean percentage of days per year is indicated by the colored dashed lines for each domain. The percentage of double tropopause events per year is shown by the black solid line.

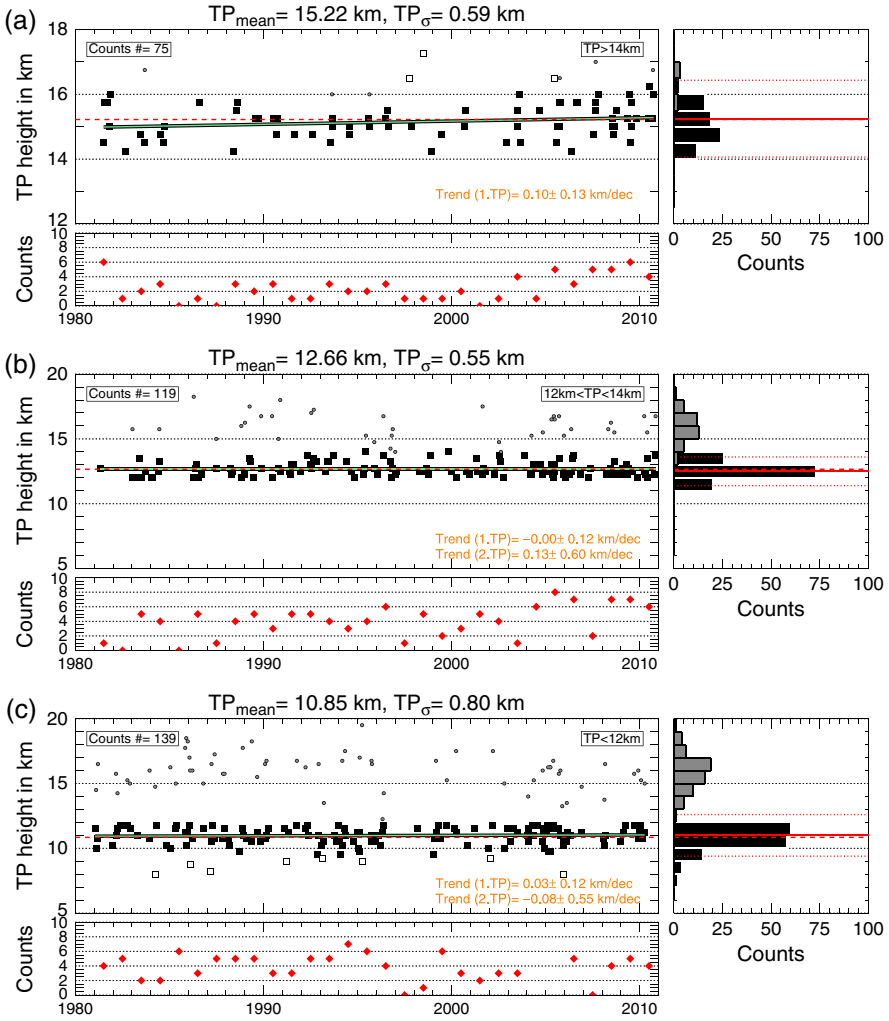

Figure 5. Tropopause height statistics over Boulder for different domains: (a) tropical domain D1 with TP > 14 km, (b) transitional domain D2 with 12 km < TP < 14 km, and (c) extratropical domain D3 with TP < 12 km. Tropopause heights outside two standard deviations around the median are considered as outliers (white squares). The counts of profiles for each year are shown as red diamonds. Linear trends and the respective 2σ limits are given for the tropopause and the double tropopauses, the linear fit for the tropopause is additionally highlighted as green line. As in Figure 3, the mean tropopause (red dashed line), median tropopause (red solid line), and two standard deviations around the median (red dotted lines) are shown.

weather.uwyo.edu/upperair/sounding.html). The mean vertical resolution of these radiosonde data is around 30 m in geopotential height around the tropopause. For each of the 12Z soundings, the height of the thermal tropopause is determined whereas some soundings are excluded since they do not reach the tropopause level. Finally, a varying amount between 273 and 348 daily observations per year is used for the statistics (Figure 4a).

[36] The mean percentage of days per year over the period 1979–2012 with tropopause heights characteristic for domain D1 is 22% and for the domains D2 and D3, 28% and 50%, respectively (Figure 4b). Note that these frequencies are based on a varying number of total amount of soundings per year (Figure 4a). Anyhow, there is no statistically significant trend in the percentage of days per year within any of these three domains over the entire period 1979–2012. Boulder therefore has not experienced a change in frequency of tropical versus extratropical air mass characteristics and thus seems to be located in a geographical region that is less strongly influenced by the tropical belt widening toward higher latitudes [*Seidel and Randel*, 2007].

3.2.2. Tropopause Height Trends for Three Different Air Mass Types

[37] Figure 5 presents the tropopause heights from Figure 3 separately for the tropical domain D1 (Figure 5a), the transitional D2 (Figure 5b), and the extratropical domain D3 (Figure 5c) from 1981 to 2011. The mean tropopause height and its standard deviation for the tropical domain D1 is 15.22 km ± 0.59 km, for the transitional domain D2 12.66 km ± 0.55 km, and for the extratropical domain D3 10.85 km ± 0.80 km.

[38] Trends in tropopause heights are separately estimated for 30 years of data representative for the three domains (black squares in Figure 5). To detect outliers in this data set, all tropopause heights which are outside two standard deviations around the median (open squares) are excluded.

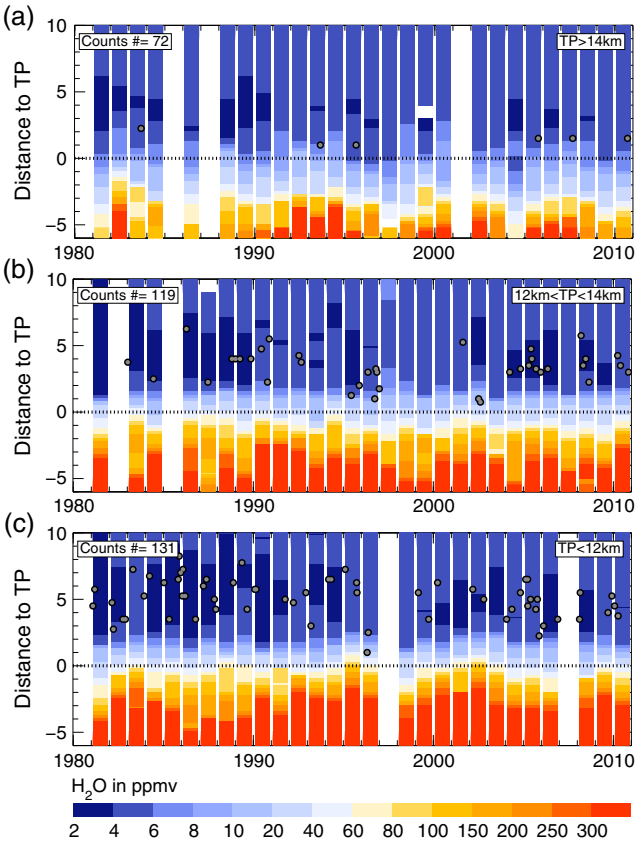

Figure 6. Annual mean water vapor in ppmv in tropopause relative coordinates for the three domains (a) D1, (b) D2, and (c) D3. Only profiles with a tropopause height within two standard deviations around the median are used for these plots (compare Figure 5). Gray dots indicate double tropopauses. Empty white columns, e.g., for the year 2001 of domain D1, indicate years with no measurements for the respective domain.

Outliers are only excluded for the tropical domain D1 and the extratropical domain D3. Due to the sampling of tropopause heights between 12 and 14 km, the transitional domain D2 should not contain any nonphysical tropopause heights. Three sonde profiles of the tropical domain D1 and eight sonde profiles of the extratropical domain D3 are detected as outliers and are excluded for further analyses. Trends were calculated by employing linear functions in the fitting algorithms. These linear fits reveal a positive trend in tropopause height of 0.10 ± 0.13 km/decade (including a 2σ uncertainty) for the tropical domain D1. Although this trend is not statistically significant at the 95% confidence level, it agrees well with the (also statistically nonsignificant) mean tropopause height trend for 1980–2004 deduced from different radiosonde stations at 40°N by *Seidel and Randel* [2006]. Trends for the two other domains D3 and D2 are also not statistically different from zero. Since the tropopause height trend of the two other domains D3 and D2 is negligibly small and the respective significance level strongly exceeds the calculated trends, the possible positive trend in tropopause height over Boulder would result from higher tropopauses of the tropical domain D1.

[39] The frequency of double tropopauses over Boulder increase with decreasing tropopause height, i.e., most double tropopauses are visible for the extratropical domain D3. This domain is most probably characterized by a second thermal tropopause which overlaps the first thermal tropopause. Furthermore, there is a seasonal cycle of double tropopauses with a higher climatological frequency in DJF (≈ domain D3) than in JJA (≈ domain D1) in agreement with other studies [*Randel et al.*, 2007; *Añel et al.*, 2008; *Peevey et al.*, 2012]. The extratropical domain D3 is characterized by a statistically nonsignificant trend in double tropopause heights. The tropopause trend statistics are repeated for the daily radiosonde data at Denver station and no significantly different results are obtained. The Denver radiosonde data also indicate statistically nonsignificant trends in tropopause height for each of the three domains (not shown).

[40] There is an increasing frequency of sonde profiles per year within the last decade, in particular, in the domains with tropical and transitional air mass characteristics D1 and D2 (Figures 5b and 5c). The influence of this uneven temporal sampling on the resulting trends in tropopause height and water vapor (presented in section 3.2.2) has been tested by randomly subsampling the sonde profiles after the year 2000 multiple times to create artificial data sets based on an even temporal sampling. The slopes of the original trends based on the uneven temporal sampling are well within the area of two standard deviations around the mean slope of multiple artificial even time series. Consequently, trends presented in this paper are not influenced by an uneven temporal

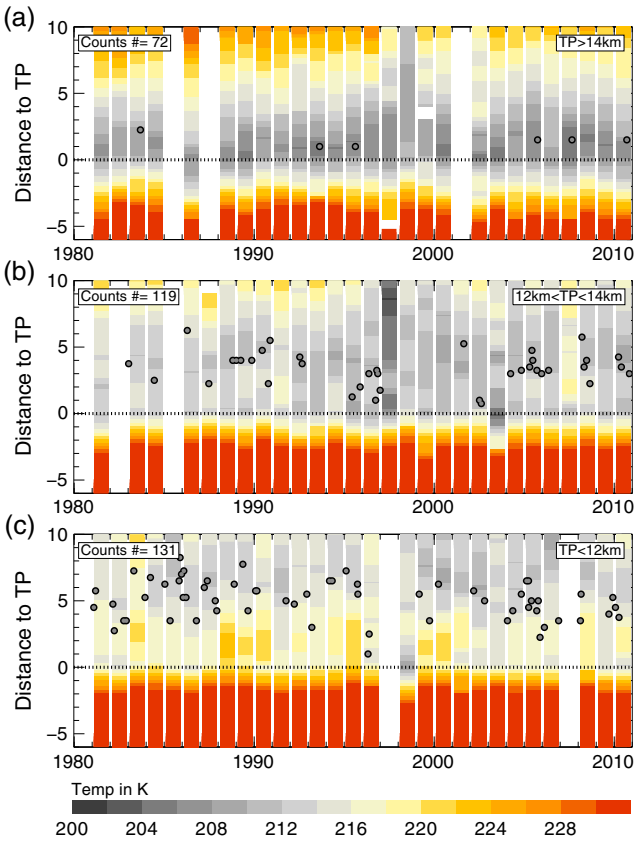

Figure 7. As Figure 6 but for temperature in K, as measured by the Boulder sondes.

sampling connected with an increasing frequency of sonde profiles within the last decade.

[41] In summary, three domains according to different tropopause height levels and air mass types can be retrieved from sonde data over Boulder. In the following, the chemical composition and temporal structure of these domains will be analyzed using FPH water vapor and temperature measurements.

3.3. UTLS Water Vapor and Temperature Structure Over Boulder

3.3.1. Water Vapor and Temperature Time Series

[42] Figure 6 shows the time series of water vapor over Boulder selected according to the three domains of tropopause height. The time series are presented in coordinates relative to the tropopause level for each sonde between –6 km below the tropopause and 10 km above the local tropopause level. The effect of averaging in tropopause relative coordinates is a more sharp vertical water vapor distribution around the tropopause for the three domains compared with averaging in sea level relative coordinates (not shown).

[43] The tropical domain D1 is characterized by the lowest mixing ratios between 5 and 10 ppmv in the vicinity of the tropopause and the extratropical domain D3 with highest mean water vapor mixing ratios of around 40 to 50 ppmv (Figures 6a and 6c). The three different domains reveal different atmospheric water vapor reservoirs. Domain D1 mainly consists of young and dry air masses above the tropopause with lowest water vapor mixing ratios characteristic for the tropical LS that are influenced by recent dehydration of the air at the cold tropical tropopause [e.g., *Fueglistaler et al.*, 2009; *Schiller et al.*, 2009]. Domain D3 is influenced by older and wetter air masses in the LS and higher water vapor mixing ratios than in domain D1. Air masses with higher water vapor in the extratropics may have experienced significant methane oxidation in the LS [e.g., *Jones and Pyle*, 1984; *Rohs et al.*, 2006]. Additionally, tropospheric intrusions [*Ploeger et al.*, 2013] or convective injections into the LS [*Ravishankara*, 2012; *Schwartz et al.*, 2013] have the potential to sporadically enhance local water vapor concentrations. Domain D2 is an in-between reservoir which is strongly influenced by the location of the subtropical jet stream connected with a seasonal cycle of the transport barrier at the tropopause [*Haynes and Shuckburgh*, 2000; *Kunz et al.*, 2011b].

[44] Temperature time series (Figure 7) also show a sharp transition across the tropopause for the tropical D1. Toward the lower tropopause domains, the temperature structure is less sharp. The extratropical domain D3 is characterized by a strong temperature fluctuation at and above the tropopause. This can be explained with the frequent double tropopause events influencing this extratropical domain D3. Connected with a double tropopause, there are single sonde profiles with a relatively high temperature between the thermal tropopause and the double tropopause. These regions indicate perturbations of the tropopause region due to exchange processes across the tropopause. For example, deep tropospheric intrusions associated with a double tropopause are connected with an intrusion of air masses characterized by a low buoyancy frequency squared characteristic for the upper troposphere [*Pan et al.*, 2009; *Homeyer et al.*, 2011]. The high temperature anomalies above the tropopause of domain D3 are also associated with double tropopause events and low buoyancy frequencies squared. In contrast, the buoyancy frequency squared above the tropopause the tropical domain D1 represents a sharp transition across the tropopause without any disturbances (not shown).

[45] Figures 6 and 7 do not show an increase in the frequency of double tropopause (gray dots) as reported by *Castanheira et al.* [2009], or even in the frequency of intrusions into the lower stratosphere. This may well be due to the limited data frequency available for this study. Sonde data profiles are analyzed, which are usually measured once a month, whereas *Castanheira et al.* [2009] use daily or twice daily radiosonde observations from a 187-station global network for the 1970–2006 period. The frequency of double tropopauses has been tested based on the daily Denver radiosonde data (Figure 4, black line). There is a statistically significant positive trend of double tropopause frequency of $4.2\% \pm 2.0\%$/decade in the period from 1979 to 2008 over Denver, whereas the annual frequency of double tropopause is decreasing from 2008 to 2012. Note that the varying number of soundings per year (Figure 4a) may have an influence on the strength of this trend. Anyhow, Boulder should also have experienced an increase in frequency of double tropopause events. However, the "limited" number of Boulder sonde profiles does not allow a reliable conclusion about the double tropopause frequency.

[46] Figures 6 and 7 demonstrate that the selection criteria according to the tropopause characteristics over Boulder are reasonable to obtain a meaningful picture of the distribution of water vapor and the thermal stratification around the tropopause. Without these selection criteria, Figure 6 would present a much more variable distribution of water vapor based on a mixture of different water vapor reservoirs around the tropopause, which may be both of tropical and extratropical nature at the same latitude. The reduction of variability of water vapor around the tropopause is particularly essential for the estimation of trends around the tropopause, which is presented in the following section.

3.3.2. Water Vapor Trends

[47] Figure 8 presents time series of Boulder sonde water vapor for the three different tropopause domains in 2 km layers around the tropopause from 2 km below to 10 km above the tropopause. For each 2 km layer, the mean water vapor (black diamonds) is calculated from the seven equidistant 0.25 km measurement points within this particular layer. The linear fits are applied to these mean water vapor measurements relative to the tropopause after excluding some outliers determined as described in section 2.4.3.

[48] There is no statistically significant trend of water vapor in the layers between –2 km below and 4 km above the tropopause for all three domains (Figure 8, fourth to sixth rows). Although the tropical domain D1 visually suggests a negative trend in water vapor in the layer below the tropopause, the resulting trend of -0.62 ± 0.99 ppmv/decade is not statistically different from zero. In these layers, the width of the 95% significance level widens toward the extratropics which may well be due to the higher variability induced by the prevailing dynamics, e.g., upward and downward variation of the tropopause and intrusions of stratospheric air masses across the tropopause as discussed

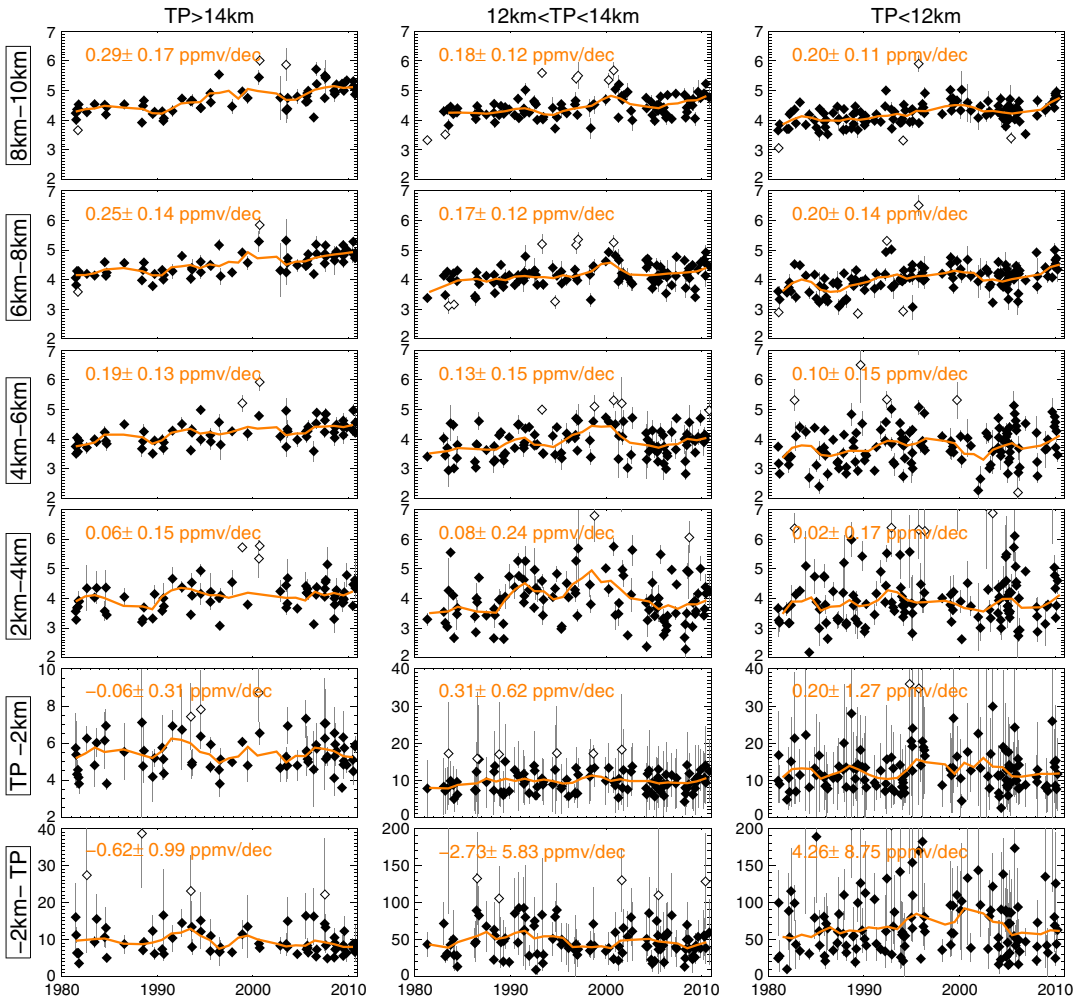

Figure 8. Water vapor trends in 2 km bins relative to the thermal tropopause for (left column) domain D1, (middle column) domain D2, and (right column) domain D3. The means of water vapor within each 2 km bin are shown as black diamonds and the respective standard deviation as gray lines. Two year running mean as orange line, outliers as white diamonds. The respective trends and significance level values are listed in orange in each panel.

in Figures 6 and 7. In contrast to prior trend analyses below 16 km [*Oltmans et al.*, 2000], variability of water vapor due to tropopause height variation is reduced in the analysis presented here. Nevertheless, uncertain trends in the extratropical UTLS still remain probably due to the remaining variability of water vapor in this region.

[49] In the layers 4 to 10 km above the tropopause (Figure 8, first to third rows), the trend in water vapor is statistically significant as expected by earlier studies on water vapor trends in the stratosphere at altitudes above 16 km [*Oltmans et al.*, 2000; *Hurst et al.*, 2011]. Here statistically significant trends are generally found in layers at or slightly above the hygropause, i.e., above the altitude where the vertical water vapor profile is characterized by a minimum (compare Figure 1). The tropical domain D1 therefore reveals statistically significant trends starting in layers 4 km above the tropopause and the extratropical domain D3 around 6 km above the tropopause.

[50] A comparison of the trends in this study, which are presented in tropopause relative coordinates and are separated for three different tropopause domains (Figure 8), with trends based on sea level relative coordinates without a respective data selection, e.g., the trends reported by *Hurst et al.* [2011], is not straightforward. In general, statistically significant trends are calculated between 0.17 ± 0.12 ppmv/decade for the 6–8 km layer (domain D2) and 0.29 ± 0.17 ppmv/decade for the 8–10 km layer (domain D1) above the tropopause in this study. *Hurst et al.* [2011] report trends based on the Boulder sonde data as growth rates which are calculated as the net change in water vapor abundance divided by the length of trend period. They find statistically significant growth rates of 0.24 ± 0.09 ppmv/decade in the 16–18 km altitude layer which increase to 0.42 ± 0.08 ppmv/decade in the 22–24 km altitude layer for the period from 1981 to 2010. Differences between our analysis and the study by *Hurst et al.* [2011] mainly result from the different trend determination method and the trends reported here and those reported by *Hurst et al.* [2011] are not directly comparable. They divided their data record into four distinct trend periods based on a statistical algorithm that detects change points in the data record. Within each period, they determined the trends

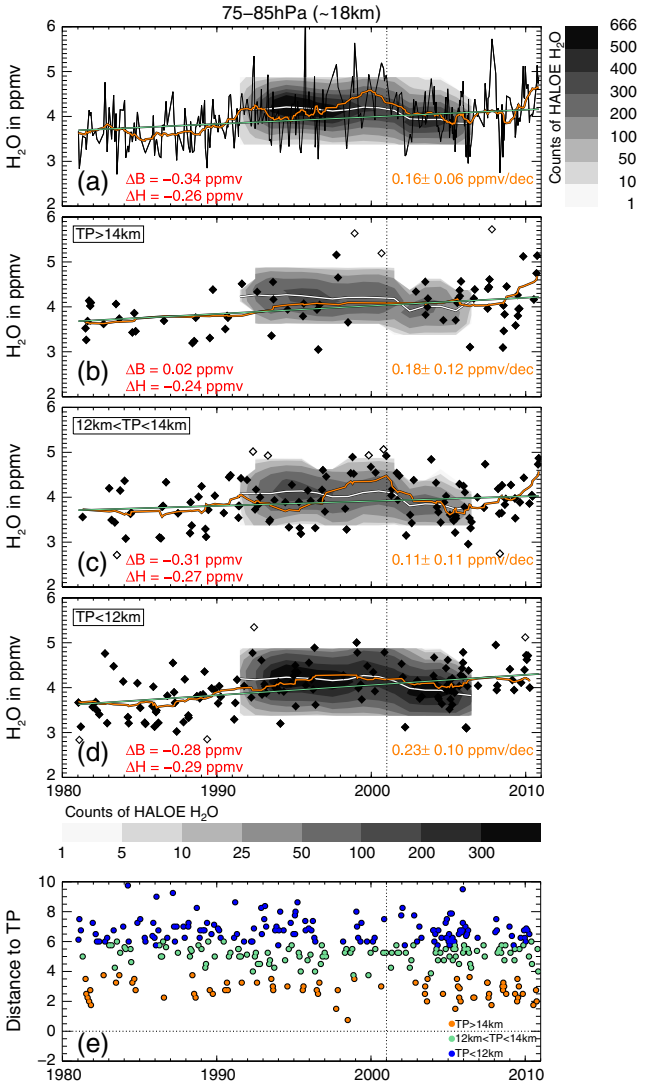

Figure 9. Water vapor trend analysis on Boulder sonde data for (a) the 75–85 hPa pressure range from 1981 to 2010 and for downsampled data into the three domains, i.e., (b) tropical domain D1, (c) transitional domain D2, and (d) extratropical domain D3. Black diamonds show water vapor means, white diamonds show outliers. Linear trend as green line, 2 year running mean as orange lines. Counts of HALOE values are gray shaded, their respective 2 year running mean is shown as white line. HALOE water vapor values are increased by the difference of mean HALOE (1993–2005) and mean Boulder sonde data (1981–2010) per altitude bin. Note different color bar ranges between Figures 9a and 9b–9d. (e) Distance to the thermal tropopause for each of the water vapor means, color coded regarding tropopause domains. Vertical black dashed line marks the year 2001. ΔB represents the difference of mean Boulder sonde water vapor between 1996–2000 and 2001–2005, ΔH represents the respective changes based on HALOE data.

using a technique of piecewise continuous fitting. Since this procedure may not work very well for the three subrecords that each contain only 25–40% of the total Boulder sonde record, using simple linear fits over all 30 years turned out to be more appropriate for long-term trend determinations in this study.

[51] A comparison between the analysis method presented in this study and conventional analyses based on sea level relative coordinates is presented in Figure 9. Here the entire Boulder water vapor data are sampled for the pressure range between 75 and 85 hPa, corresponding approximately to an altitude level of 18 km in the lower stratosphere. For this pressure range, a trend in water vapor of 0.16 ± 0.06 ppmv/decade is obtained (Figure 9a). A separation of the data within this 75–85 hPa pressure range according to the three tropopause domains reveals a highest trend in water vapor of 0.23 ± 0.10 ppmv/decade for the extratropical domain D3 (Figure 9d) and a trend of 0.18 ± 0.12 ppmv/decade for the tropical domain D1 (Figure 9b).

[52] The difference of trends for data within the full pressure range between 75 and 85 hPa and those data separated into the three domains may well be due to the fact that the data within the 75–85 hPa pressure range are close to the tropopause for the tropical domain, i.e., roughly between 2 and 4 km above the tropopause, whereas the data for the domain D3 in the same pressure range are higher in the stratosphere between 6 and 10 km above the tropopause (see orange and blue dots in Figure 9e). Generally, the magnitude of trends of water vapor increases with altitude (see Figure 8 and *Oltmans et al.* [2000] or *Hurst et al.* [2011]). This is one reason for the higher water vapor trend within the extratropical domain of the 75–85 hPa example. Furthermore, a conventional analysis in a pressure range of 75–85 hPa does contain water vapor data of different atmospheric reservoirs with different background values. Water vapor measured in the vicinity of the tropopause corresponding to tropical tropopause height characteristics is mixed with measurements deeper in the stratosphere relative to a lower tropopause with extratropical height characteristics (Figure 9e). The difference of the altitude levels relative to the tropopause may affect the strength in statistical significance of trends for the two domains.

[53] The increase of water vapor until 2000 and the decrease in the following years have been described in literature [e.g., *Randel et al.*, 2006; *Scherer et al.*, 2008] and are visible for the entire pressure range of 75–85 hPa (Figure 9a) [see also *Solomon et al.*, 2010]. Here the change in mean Boulder sonde water vapor mixing ratio between 1996–2000 and 2001–2005 is quantified as ΔB = –0.34 ppmv. This drop in mean water vapor is also visible after dividing the data into the three domains with ΔB = –0.31 ppmv for the transitional domain D2 and ΔB = –0.28 ppmv for the extratropical domain D3. A quantification of the water vapor change between 1996–2000 and 2001–2005 is difficult for the tropical domain D1 because of lacking sonde profiles around 2000 after subsampling the data set (Figure 9b). Therefore, HALOE data are also considered when addressing the drop in water vapor around 2000 and the respective water vapor change within the three domains. HALOE data principally confirm the water vapor change throughout the entire 30 years as observed by the Boulder sondes except for

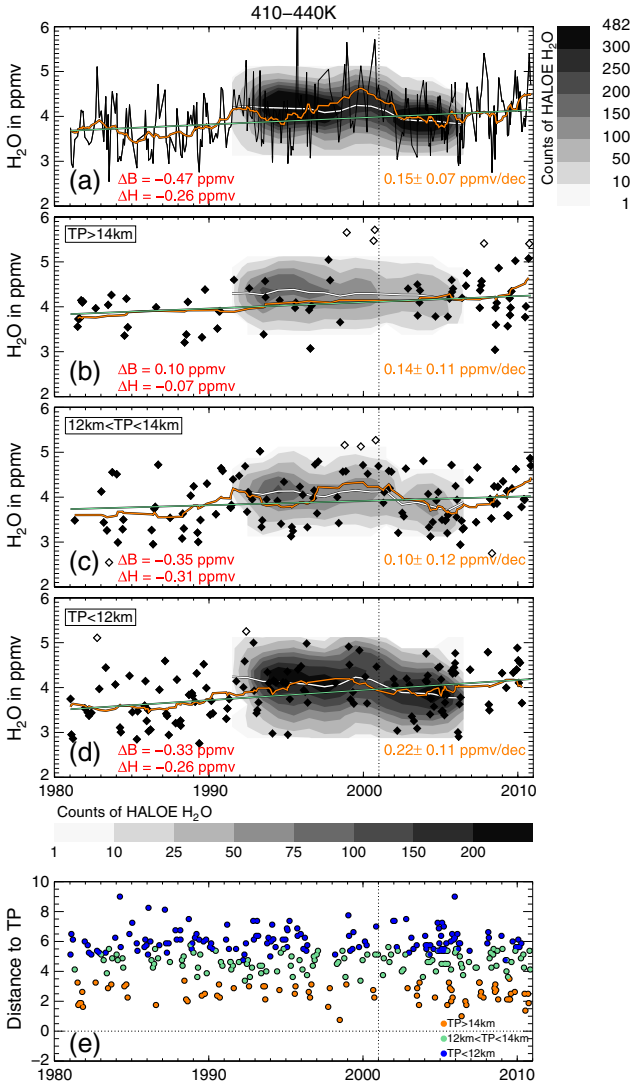

Figure 10. Same as Figure 9 but for water vapor trends within the isentropic range 410–440 K.

the well-known difference between the mean HALOE and mean Boulder sonde water vapor data [e.g., *Randel et al.*, 2004; *Solomon et al.*, 2010]. Based on HALOE data, the water vapor change between 1996–2000 and 2001–2005 is ΔH = –0.26 ppmv for the entire 75–85 hPa pressure range. It does not significantly vary from that value after dividing the data into the three domains. The sensitivity of the change in water vapor around 2000 on the different domains is further tested for the 50–75 hPa and 85–100 hPa pressure ranges which are well above the tropopause. Both pressure ranges do not show a significant different intensity of the water vapor drop around 2000 within the three domains as well (not shown).

[54] In the following, the sensitivity of the change in mean water vapor between 1996–2000 and 2001–2005 is also tested for different isentropic ranges (see Figure10 and Table 1). The isentropic range between 410 and 440 K is within the lower stratosphere and is not influenced by tropopause height fluctuations (see Figure 2). It is an isentropic range that is strongly influenced by dynamics of the lower branch of the Brewer Dobson circulation and quasi-horizontal transport of air masses from the tropics above the tropopause and below the lower edge of the tropical pipe to the extratropics [*Bönisch et al.*, 2009; *Rosenlof et al.*, 1997].

[55] Within the isentropic range 410–440 K, there is a change in mean water vapor around 2000 within the transitional domain D2 and extratropical domain D3 (Figures 10c and 10d), whereas the change is hardly visible for the tropical domain D1 (Figure 10b). Largest changes in mean water vapor are found for the transitional domain with ΔB = –0.35 ppmv and ΔH = –0.31 ppmv. The respective values for the tropical domain D1, i.e., ΔB = 0.10 ppmv and ΔH = –0.07 ppmv are much smaller. Hereby, the positive sign of the mean change based on Boulder sonde data should not be interpreted as physical because of the lacking sonde profiles around 2000 in that domain. A subsampling of data into 410–420 K, 420–430 K, and 430–440 K does show this strengthening of the water vapor drop around 2000 toward the extratropics for each isentropic range without any dependence on the height of the isentropic level (see Table 1).

[56] A link between the water vapor change in the years around 2000 and dynamics in the lower stratosphere above the subtropical jet stream such as quasi-isentropic transport through the shallow branch of the Brewer-Dobson circulation can be motivated. This may be an additional explanation besides temperature and water vapor feedbacks based on freeze drying at the tropical tropopause as suggested by *Randel et al.* [2006], who attributed the sudden drop in stratospheric water vapor in 2001 to anomalously low temperatures at the tropical cold point tropopause (see also section 4.3 for a further discussion).

3.4. Radiative Calculations Based on H_2O Trends

[57] Water vapor changes in the tropopause region affect fluxes of longwave and shortwave radiation and can thereby influence the temperature in the stratosphere and troposphere and thus climate [*Forster and Shine*, 2002; *Solomon et al.*, 2010]. In the following, radiative effects of water vapor changes in the tropopause region over Boulder are investigated. In particular, the radiative forcing at the tropopause

Table 1. Change in Mean Water Vapor Mixing Ratio Between 1996–2000 and 2001–2005 in ppmv for Different Isentropic Ranges Between 410 and 440 K[a]

	410–420 K	420–430 K	430–440 K	410–440 K
All	ΔB = –0.54, ΔH = –0.21	ΔB = –0.48, ΔH = –0.28	ΔB = –0.34, ΔH = –0.30	ΔB = –0.47, ΔH = –0.26
D1 (TP > 14 km)	ΔB = –0.10, ΔH = –0.00	ΔB = –0.37, ΔH = –0.18	ΔB = 0.01, ΔH = –0.05	ΔB = –0.10, ΔH = –0.07
D2 (12 km < TP < 14 km)	ΔB = –0.12, ΔH = –0.25	ΔB = –0.49, ΔH = –0.28	ΔB = –0.33, ΔH = –0.27	ΔB = –0.35, ΔH = –0.31
D3 (TP < 12 km)	ΔB = –0.18, ΔH = –0.30	ΔB = –0.34, ΔH = –0.21	ΔB = –0.16, ΔH = –0.27	Δ*B* = –0.33, ΔH = –0.26

[a] ΔB represents the mean water vapor change based on Boulder sonde data and ΔH the mean change based on HALOE data. ΔB for domain D1 should not be taken as physical since the respective means are based on low statistics, i.e., between two and six values.

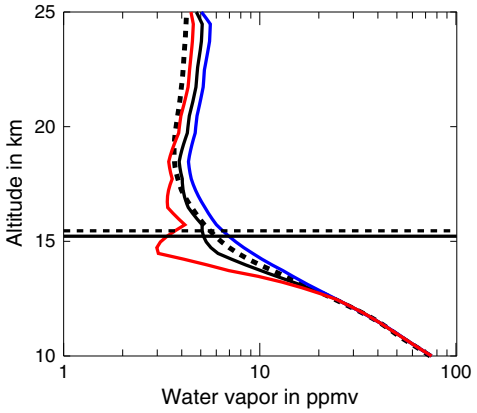

Figure 11. Reference profile of water vapor in ppmv for the year 1981 (black dashed lines) calculated for all sonde profiles within this year with a tropopause higher than 14 km (tropical domain D1). The expected profile after 30 years (black solid line) includes the proposed mean trend taken from Figure 8. Trend uncertainties are considered by calculating upper limit and lower limit trend profiles by adding and subtracting the 2σ uncertainty (blue and red solid curves). The 30 year mean height of the tropopause (horizontal black solid line) and the mean tropopause height for the year 1981 (black dashed line) are shown.

since 1981 is computed under the assumption that the water vapor changes around the tropopause are described by the mean trends determined in this study, even though these trends carry large uncertainties and are not statistically different from zero. Although, the trends reported here in the vicinity of the tropopause are uncertain, it is of interest to evaluate the potential climate impacts of these changes by calculating the radiative forcing over Boulder. The radiative effects of water vapor at the tropopause over Boulder are therefore investigated based on water vapor trends with regard to their respective observed uncertainty limits. In the following, the radiative impact is assessed for trends retrieved for the tropical domain D1 since this domain is characterized by less water vapor variability than the other two domains.

[58] Figure 11 shows the mean water vapor profile for the year 1981 and three mean profiles which are expected after 30 years including trends for the respective height levels. First, there is the water vapor profile based on the mean 30 year trend. Second, two further profiles are calculated, which include the respective 2σ uncertainties around the mean trend, i.e., the upper limit and lower limit trend profiles which are expected after 30 years. The maximum and minimum radiative forcing by these water vapor changes will be determined from the trends and their uncertainties.

[59] Using the radiation code described in section 2, the 1981 water vapor trend profile is taken as a reference profile and the three different mean trend profiles as perturbation profiles. Following *Forster and Shine* [1999, 2002], stratospheric temperatures are adjusted to these particular perturbations using the fixed-dynamical-heating assumption to quantify the stratospheric-adjusted radiative forcing. Figure 12 presents the results of the three sets of radiative transfer calculations. The radiative forcing of water vapor at the tropopause over Boulder is estimated about -0.14 ± 0.49 W/m^2. This radiative forcing is connected with a temperature change in the stratosphere which is positive for the mean and lower limit trends, but may also be negative for the upper limit trend (see Figure 12, right).

[60] A globally averaged radiative forcing of 0.29 W/m^2 for the 1980–2000 period was reported by *Forster and Shine* [2002] under the assumption that the trend at 30 km is representative for the entire region downward to the tropopause. Similarly, *Solomon et al.* [2010] assumed a 1 ppmv water vapor increase in the entire region above the tropopause between 1980 and the 1996–2000 period and a globally averaged radiative forcing of 0.24 W/m^2 including a stratospheric adjustment was obtained. At the latitude of the Boulder sonde station (40°N), a net radiative forcing of 0.35 W/m^2 was found due to stratospheric water vapor changes [*Forster and Shine*, 2002]. This local value of radiative effect of water vapor near the tropopause over Boulder is close to the upper limit of radiative forcing. This upper limit

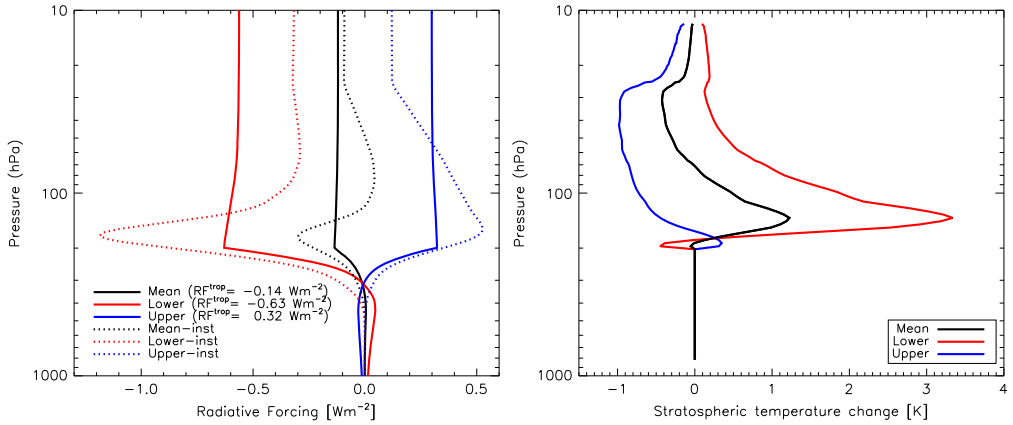

Figure 12. Radiative effects of the mean trend profiles as shown in Figure 11. (left) Instantaneous forcings (dotted lines) and radiative forcings after stratospheric adjustment (solid lines) in W/m^2 based on the perturbation as given by the three mean water vapor profiles including the 30 year trend (solid lines in Figure 11). (right) Stratospheric temperature change resulting from the three perturbations.

radiative forcing corresponds to a net water vapor increase in the entire altitude range above the tropopause of ≈1–2 ppmv within 30 years (see Figure 11).

[61] Several studies emphasized the large sensitivity of surface climate to changes of the temperature and composition in the UTLS [*Solomon et al.*, 2010; *Riese et al.*, 2012]. An increase (decrease) in water vapor in the lower stratosphere is linked with a surface warming (cooling). The 30 year decreasing trend in water vapor near the tropopause would therefore cause a cooling of the surface, but like the water vapor change itself, the cooling trend is not statistically significant. However, calculations of the upper limit and lower limit trend profiles based on the 2σ uncertainties predict radiative forcings with uncertain signs. Radiative effects of water vapor are particularly sensitive to trend uncertainties near the tropopause.

4. Discussion and Conclusions

[62] The Boulder balloon sonde data set for the period 1981–2011 is used to study variability and trends of water vapor in the vicinity of the thermal tropopause. The study focuses on the UTLS at 40°N from 2 km below the tropopause up to 10 km above the tropopause, a region which comprises geopotential heights in the range from approximately 13 to 25 km in JJA and 9 to 21 km in DJF. The data set is consistently presented here in coordinates relative to the local thermal tropopause, and trends in water vapor are calculated in 2 km layers relative to the tropopause.

[63] For the investigation, the sonde data are separated into three different sets according to the tropopause height and air mass types: a tropical domain D1 with TP > 14 km, an extratropical domain D3 with TP < 12 km, and a transitional domain D2 with tropopauses in between, i.e., 12 km < TP < 14 km. In this way, high tropopause heights characteristic for the tropics are separated from lower tropopause heights characteristic for the extratropics. Different water vapor reservoirs are identified by this methodology. Through the separation according to tropopause domains, variability of water vapor at the tropopause is reduced which would otherwise result from mixing of low water vapor mixing ratios characteristic for the tropical tropopause with higher mixing ratios characteristic for the extratropical tropopause at the same geographical latitude 40°N.

4.1. Water Vapor Trend Quantification

[64] Earlier trend studies based on the Boulder balloon sonde data set [e.g., *Oltmans et al.*, 2000; *Scherer et al.*, 2008; *Hurst et al.*, 2011] are extended to altitudes below 16 km. A comparison of the tropopause-based analysis of water vapor in the layer around the tropopause with existing sea level-based analyses in the tropopause region between 10 and 12 km [see *Oltmans and Hofmann*, 1995, Figure 2] shows that the uncertainty of the trends is reduced through the separation of the data set into three tropopause domains. This reduction may well be due to the analysis method utilized here for trend determination in the UTLS which largely excludes biases from the mixing of different water vapor reservoirs. Despite the bias reductions, the trends are still uncertain at altitudes roughly below the hygropause, representing the water vapor minimum around 3.5 km above the thermal tropopause. Water vapor remains particularly variable around the tropopause in the extratropical domain D3 and trends are statistically nonsignificant.

[65] Despite the long data record of over 30 years, Boulder sonde data are a set of low-frequency measurements at one single station. The separation of these data into three subdomains clearly reduces the data population of each subrecord, i.e., based on our dynamical criterion, the number of data is reduced in each of the three domains by around 60–70%. On the one hand, taking the entire record of sonde data, i.e., at least 333 soundings, reveals statistically nonsignificant trends between –2 and 4 km around the tropopause probably based on the nature of the highly variable trace gas water vapor. Different water vapor reservoirs are apparent in the total Boulder data set and the analysis of these reservoirs together clearly increases the variability of water vapor at the tropopause. Subsetting the small data set available into three subsets reduces geophysical variability, but the smaller size of each subset results in a statistically nonsignificant trend determination.

[66] After all, this discussion underlines the need of higher-frequency measurements of water vapor at more sites over the globe. These sites should probably be in regions which are less influenced by the dynamics of jet streams to avoid a sampling of different water vapor reservoirs in particular at the tropopause.

4.2. Radiative Impacts of Water Vapor

[67] Based on the observed trends of the tropical domain D1, the possible radiative effects of water vapor changes around the tropopause over Boulder are estimated. A mean change in water vapor of -0.62 ± 0.99 ppmv/decade in the 2 km layer below the tropopause and a rather vanishing change in water vapor of -0.06 ± 0.31 ppmv/decade in the 2 km layer above the tropopause (see Figure 8, left) would impart a radiative forcing of uncertain sign at the tropopause -0.14 ± 0.49 W/m^2. This means the possible radiative forcing at the tropopause may be positive or negative, dependent on the sign of the respective trend there. If there were a statistically significant trend of water vapor at the tropopause, the resulting radiative effect would not be higher than 0.32 W/m^2 or lower than –0.63 W/m^2. For comparison, the global mean radiative forcing of carbon dioxide is estimated about 0.50 W/m^2 since 1980 [*Forster and Shine*, 1999]. The radiative forcing of water vapor and its uncertainties presented here can be seen as lower limits. The calculation is based on trend uncertainties concerning the tropical domain D1 with tropical air mass types. The inclusion of trend uncertainties of the D3 and D2 domains would further increase the uncertainties of radiative forcing of water vapor presented here.

[68] So far it has not been possible to determine a statistically significant trend of water in the tropopause region. It is not proven that the strength of water vapor increase observed at higher altitudes deeper in the stratosphere may also be appropriate for levels close to the tropopause. In particular, the value of the water vapor trend is increasing from the tropopause toward higher altitudes in the stratosphere. An assumption of a constant value of water vapor trend in the entire region above the tropopause level, e.g., 1 ppmv between 1980 and 2000, may induce substantial biases in radiative forcing, in particular at the tropopause.

[69] This study shows that radiative forcing of water vapor is particularly sensitive to the strength and sign of trends around the level of the tropopause. A positive trend of water vapor clearly results in a positive radiative effect at the tropopause and vice versa. This underlines the role of water vapor in the tropopause region as a major uncertainty in the assessment of radiative forcing and the resulting feedback in global warming. This is particular relevant since the response for a given stratospheric water vapor change on radiative forcing of surface climate peaks near the tropopause [*Solomon et al.*, 2010].

4.3. Water Vapor Variability

[70] Several studies emphasize a change in water vapor mixing ratio in the year 2000 between 16 and 28 km, after an increase in water vapor at the end of the 1990s, a decrease follows until around 2005 [*Randel et al.*, 2006; *Hurst et al.*, 2011]. The change in mean water vapor between 1996–2000 and 2001–2005 is visible for all three domains in different pressure ranges between 50 and 100 hPa. Thus, the intensity of this drop in mean water vapor within different pressure ranges is not sensitive to the subsampling into three domains. In contrast, an analogous study based on potential temperature ranges between 410 and 440 K in the lower stratosphere reveals an intensified change of mean water vapor around 2000 toward the extratropical domains. Based on isentropes, there is hardly a change of mean water vapor for the tropical domain D1. This is observed both for Boulder sonde data and HALOE satellite data.

[71] *Randel et al.* [2006] suggest that the decrease in water vapor after 2000 is consistent with an increase in the mean tropical upwelling as part of the Brewer-Dobson circulation and the resulting cooling of the tropical lower stratosphere. This circulation in the stratosphere is characterized by a mean upwelling near the tropical tropopause which is balanced by a mean downwelling in the extratropics poleward of 40°N [e.g., *Holton et al.*, 1995; *Rosenlof*, 1995; *Butchart et al.*, 2006]. The enhanced tropical upwelling may cause the lower temperatures and lower water vapor near the tropical tropopause which are observed after 2000 [*Randel et al.*, 2006]. *Bönisch et al.* [2011] provide evidence that the observed increase in tropical upwelling may be attributed to a change in the Brewer-Dobson circulation pattern. In particular, the increased upwelling has the potential to trigger an intensified tracer transport from the tropical into the extratropical LS which is part of the shallow branch of the Brewer-Dobson circulation.

[72] We therefore hypothesize that the acceleration of the shallow branch of the Brewer-Dobson circulation may influence the strength of the kink in water vapor around the year 2000 with an intensified tracer transport on its pathway from the tropics into the extratropical LS. The stronger kink in the extratropical domain D3 compared with the tropical domain D1 that is observed on isentropic surfaces may well be influenced by the quasi-horizontal transport of younger and dryer air from low to high latitudes by the shallow branch of the Brewer-Dobson circulation. The latitude of the Boulder sonde station is characterized by an enhanced quasi-horizontal transport up to 450 K during summer compared with winter [*Ploeger et al.*, 2013]. The seasonality in meridional tracer transport may additionally contribute to the varying strengths of water vapor kinks after 2000 in the three domains with different air mass types over Boulder.

[73] The reader should keep in mind that the presented analysis of the UTLS is representative for a particular geographical latitude at 40°N and longitude at –105°W. After all, this analysis underlines the sensitivity of water vapor variability to dynamical and chemical processes in the tropopause region. Large uncertainties of trends and radiative forcing of water vapor therefore remain in the tropopause region, a region of key importance for radiative forcing and understanding climate change in the atmosphere. In the future, a tropopause-based analysis of trends in water vapor in the UTLS may be extended to a larger geographical region. *Gettelman et al.* [2010] presented a multimodel assessment of the UTLS and calculated trends of simulated ozone and water vapor fields globally from 1960 to 2100. How well the models used in this study reproduce the observed trends and their uncertainties in the tropopause region over Boulder from 1981 to 2011 may contribute to the evaluation of the capability of the models to reproduce UTLS features in the subtropics and their impact on surface climate.

[74] **Acknowledgments.** The results of this analysis are to some extent supported by a funding for A. Kunz from the European Union Seventh Framework Programme (FP7/2007–2013) under grant agreement 299666, in particular, the Marie Curie Fellowship "Dynamical processes in the tropopause region and their impact on the distribution of atmospheric trace gases" (PROTRO). V. Homonnai and I. M. Jánosi are partially supported by the Hungarian Science Foundation under grant OTKA NK100296. A. Rap and P. M. Forster acknowledge funding through NERC grants NE/G005109/1 and NE/J004723/1. Many thanks to the ECMWF for providing the ERA-Interim reanalysis data and to L. Oolman for providing radiosonde data at Denver station. We are also grateful to H. Wernli and C. M. Grams for helpful discussions. Finally, we would like to thank two anonymous reviewers for their constructive criticisms that helped to improve the quality of the paper.

References

Añel, J. A., J. C. Antuña, L. de la Torre, J. M. Castanheira, and L. Gimeno (2008), Climatological features of global multiple tropopause events, *J. Geophys. Res.*, *113*, D00B08, doi:10.1029/2007JD009697.

Birner, T., A. Dörnbrack, and U. Schumann (2002), How sharp is the tropopause at midlatitudes?, *Geophys. Res. Lett.*, *29*(14), 1700, doi:10.1029/2002GL015142.

Birner, T. (2006), Fine-scale structure of the extratropical tropopause region, *J. Geophys. Res.*, *111*, D04104, doi:10.1029/2005JD006301.

Bönisch, H., A. Engel, J. Curtius, Th. Birner, and P. Hoor (2009), Quantifying transport into the lowermost stratosphere using simultaneous in-situ measurements of SF_6 and CO_2, *Atmos. Chem. Phys.*, *9*, 5905–5919.

Bönisch, H., A. Engel, Th. Birner, P. Hoor, D. W. Tarasick, and E. A. Ray (2011), On the structural changes in the Brewer-Dobson circulation after 2000, *Atmos. Chem. Phys.*, *11*, 3937–3948, doi:10.5194/acp-11-3937-2011.

Butchart, N., et al. (2006), Simulations of anthropogenic change in the strength of the Brewer-Dobson circulation, *Clim. Dyn.*, *27*, 727–741, doi:10.1007/s00382-006-0162-4.

Castanheira, J. M., J. A. Añel, C. A. F. Marques, J. A. Antuña, M. L. R. Liberato, L. de la Torre, and L. Gimeno (2009), Increase of upper troposphere/lower stratosphere wave baroclinicity during the second half of the 20th century, *Atmos. Chem. Phys.*, *9*, 9143–9153.

Dee, D. P., et al. (2011), The ERA-Interim re-analysis: Configuration and performance of the data assimilation system, *Q. J. R. Meteorol. Soc.*, *137*, 553–597, doi:10.1002/qj.828.

Edwards, J. M., and A. Slingo (1996), Studies with a flexible new radiation code: I. Choosing a configuration for a large scale model, *Q. J. R. Meteorol. Soc.*, *122*, 689–720, doi:10.1002/qj.49712253107.

Forster, P. M. de F., and K. P. Shine (1997), Radiative forcing and temperature trends from stratospheric ozone changes, *J. Geophys. Res.*, *102*(D9), 10,841–10,855.

Forster, P. M. de F., and K. P. Shine (1999), Stratospheric water vapour changes as a possible contributor to observed stratospheric cooling, *Geophys. Res. Lett.*, *26*(21), 3309–3312, doi:10.1029/1999GL010487.

Forster, P. M. de F., and K. P. Shine (2002), Assessing the climate impact of trends in stratospheric water vapor, *Geophys. Res. Lett.*, *29*(6), 1086, doi:10.1029/2001GL013909.

Fueglistaler, S., A. E. Dessler, T. J. Dunkerton, I. Folkins, Q. Fu, and P. W. Mote (2009), Tropical tropopause layer, *Rev. Geophys.*, *47*, RG1004, doi:10.1029/2008RG000267.

Gettelman, A., et al. (2010), Multimodel assessment of the upper troposphere and lower stratosphere: Tropics and global trends, *J. Geophys. Res.*, *115*, D00M08, doi:10.1029/2009JD013638.

Grise, K. M., D. W. J. Thompson, and T. Birner (2010), A global survey of static stability in the stratosphere and upper troposphere, *J. Clim.*, *23*, 2275–2292, doi:10.1175/2009JCL13369.1.

Grooß, J.-U., and J. M. Russell III (2005), Technical note: A stratospheric climatology for O_3, H_2O, CH_4, NO_x, HCl and HF derived from HALOE measurements, *Atmos. Chem. Phys.*, *5*, 2797–2807.

Haynes, P., and E. Shuckburgh (2000), Effective diffusivity as a diagnostic of atmospheric transport 2. Troposphere and lower stratosphere, *J. Geophys. Res.*, *105*(D18), 22,795–22,810.

Hoinka, K. P. (1997), The tropopause: Discovery, definition and demarcation, *Meteorol. Z.*, *6*, 281–303.

Holton, J. R., P. H. Haynes, M. E. McIntyre, A. R. Douglass, R. B. Rood, and L. Pfister (1995), Stratosphere-troposphere exchange, *Rev. Geophys.*, *33*, 403–440.

Homeyer, C. R., K. P. Bowman, L. L. Pan, E. L. Atlas, R.-S. Gao, and T. L. Campos (2011), Dynamical and chemical characteristics of tropospheric intrusions observed during START08, *J. Geophys. Res.*, *116*, D06111, doi:10.1029/2010JD015098.

Hurst, D. F., S. J. Oltmans, H. Vömel, K. H. Rosenlof, S. M. Davis, E. A. Ray, E. G. Hall, and A. F. Jordan (2011), Stratospheric water vapor trends over Boulder, Colorado: Analysis of the 30 year Boulder record, *J. Geophys. Res.*, *116*, D02306, doi:10.1029/2010JD015065.

Jones, R. L., and J. A. Pyle (1984), Observations of CH_4 and N_2O by the NIMBUS 7 SAMS: A comparison with in situ data and two-dimensional numerical model calculations, *J. Geophys. Res.*, *89*, 3D1644, doi:10.1029/JD089iD04p05263.

Kley, D., E. J. Stone, W. R. Henderson, J. W. Drummond, W. J. Harrop, A. L. Schmeltekopf, T. L. Thompson, and R. H. Winkler (1979), In situ measurements of the mixing ratio of water vapor in the stratosphere, *J. Atmos. Sci.*, *36*, 2513–2524.

Kley, D., A. L. Schmeltekopf, K. Kelly, R. H. Winkler, T. L. Thompson, and M. McFarland (1982), Transport of water through the tropical tropopause, *Geophys. Res. Lett.*, *9*(6), 617–620.

Kunz, A., P. Konopka, R. Müller, L. L. Pan, C. Schiller, and F. Rohrer (2009), High static stability in the mixing layer above the extratropical tropopause, *J. Geophys. Res.*, *114*, D16305, doi:10.1029/2009JD011840.

Kunz, A., P. Konopka, R. Müller, and L. L. Pan (2011a), Dynamical tropopause based on isentropic potential vorticity gradients, *J. Geophys. Res.*, *116*, D01110, doi:10.1029/2010JD014343.

Kunz, A., L. L. Pan, P. Konopka, D. E. Kinnison, and S. Tilmes (2011b), Chemical and dynamical discontinuity at the extratropical tropopause based on START08 and WACCM analyses, *J. Geophys. Res.*, *116*, D34302, doi:10.1029/2011JD016686.

Oltmans, S. J., and D. J. Hofmann (1995), Increase in lower-stratospheric water vapour at a mid-latitude northern hemispheric site from 1981 to 1994, *Nature*, *374*, 146–149.

Oltmans, S. J., H. Vömel, D. J. Hofmann, K. H. Rosenlof, and D. Kley (2000), The increase in stratospheric water vapor from balloonborne, frostpoint hygrometer measurements at Washington, D.C., and Boulder, Colorado, *Geophys. Res. Lett.*, *27*(21), 3453–3456, doi:10.1029/2000GL012133.

Pan, L. L., W. J. Randel, J. C. Gille, W. D. Hall, B. Nardi, S. Massie, V. Yudin, R. Khosravi, P. Konopka, and D. Tarasick (2009), Tropospheric intrusions associated with the secondary tropopause, *J. Geophys. Res.*, *114*, D10302, doi:10.1029/2008JD011374.

Pan, L. L., and L. A. Munchak (2011), Relationship of cloud top to the tropopause and jet structure from CALIPSO data, *J. Geophys. Res.*, *116*, D12201, doi:10.1029/2010JD015462.

Peevey, T. R., J. C. Gille, C. E. Randall, and A. Kunz (2012), Investigation of double tropopause spatial and temporal global variability utilizing HIRDLS temperature observations, *J. Geophys. Res.*, *117*, D01105, doi:10.1029/2011JD016443.

Ploeger, F., G. Günther, P. Konopka, S. Fueglistaler, R. Müller, C. Hoppe, A. Kunz, R. Spang, J.-U. Grooß, and M. Riese (2013), Horizontal water vapor transport in the lower stratosphere from subtropics to high latitudes during boreal summer, *J. Geophys. Res. Atmospheres*, *118*, 8111–8127, doi:10.1002/jgrd.50636.

Randel, W. J., F. Wu, S. Oltmans, K. Rosenlof, and G. E. Nedoluha (2004), Interannual changes of stratospheric water vapor and correlations with tropical tropopause temperatures, *J. Atmos. Sci.*, *61*, 2133–2148.

Randel, W. J., F. Wu, H. Vömel, G. E. Nedoluha, and P. Forster (2006), Decreases in stratospheric water vapor after 2001: Links to changes in the tropical tropopause and the Brewer-Dobson circulation, *J. Geophys. Res.*, *111*, D12312, doi:10.1029/2005JD006744.

Randel, W. J., D. J. Seidel, and L. L. Pan (2007), Observational characteristics of double tropopauses, *J. Geophys. Res.*, *112*, D07309, doi:10.1029/2006JD007904.

Ravishankara, A. R. (2012), Water vapor in the lower stratosphere, *Science*, *337*, 809–810.

Riese, M., F. Ploeger, A. Rap, B. Vogel, P. Konopka, M. Dameris, and P. Forster (2012), Impact of uncertainties in atmospheric mixing on simulated UTLS composition and related radiative effects, *J. Geophys. Res.*, *117*, D16305, doi:10.1029/2012JD017751.

Röckmann, T., J.-U. Grooß, and R. Müler (2004), The impact of anthropogenic chlorine emissions, stratospheric ozone change and chemical feedbacks on stratospheric water, *Atmos. Chem. Phys.*, *4*, 693–699.

Rohs, S., C. Schiller, M. Riese, A. Engel, U. Schmidt, T. Wetter, I. Levin, T. Nakazawa, and S. Aoki (2006), Long-term changes of methane and hydrogen in the stratosphere in the period 1978–2003 and their impact on the abundance of stratospheric water vapor, *J. Geophys. Res.*, *111*, D14315, doi:10.1029/2005JD006877.

Rosenlof, K. H. (1995), Seasonal cycle of the residual mean meridional circulation in the stratosphere, *J. Geophys. Res.*, *100*(D3), 5173–5191, doi:10.1029/94JD03122.

Rosenlof, K. H., A. F. Tuck, K. K. Kelly, J. M. Russell III, and M. P. McCormick (1997), Hemispheric asymmetries in water vapor and inferences about transport in the lower stratosphere, *J. Geophys. Res.*, *102*(D11), 13,213–13,234, doi:10.1029/97JD00873.

Rosenlof, K. H., et al. (2001), Stratospheric water vapor increases over the past half-century, *Geophys. Res. Lett.*, *28*(7), 1195–1198, doi:10.1029/2000GL012502.

Rosenlof, K. H., and G. C. Reid (2008), Trends in the temperature and water vapor content of the tropical lower stratosphere: Sea surface connection, *J. Geophys. Res.*, *113*, D06107, doi:10.1029/2007JD009109.

Sausen, R., and B. D. Santer (2003), Use of changes in tropopause height to detect human influences on climate, *Meteorol. Z.*, *12*, 131–136.

Scherer, M., H. Vömel, S. Fueglistaler, S. J. Oltmans, and J. Staehelin (2008), Trends and variability of midlatitude stratospheric water vapour deduced from the re-evaluated Boulder balloon series and HALOE, *Atmos. Chem. Phys.*, *8*, 1391–1402.

Schiller, C., J.-U. Grooß, P. Konopka, F. Plöger, F. H. Silva dos Santos, and N. Spelten (2009), Hydration and dehydration at the tropical tropopause, *Atmos. Chem. Phys.*, *9*, 9647–9660.

Schwartz, M. J., W. G. Read, M. L. Santee, N. J. Livesey, L. Froidevaux, A. Lambert, and G. L. Manney (2013), Convectively injected water vapor in the north American summer lowermost stratosphere, *Geophys. Res. Lett.*, *40*, 2316–2321, doi:10.1002/grl.50421.

Seidel, D. J., and W. J. Randel (2006), Variability and trends in the global tropopause estimated from radiosonde data, *J. Geophys. Res.*, *111*, D31101, doi:10.1029/2006JD007363.

Seidel, D. J., and W. J. Randel (2007), Recent widening of the tropical belt: Evidence from tropopause observations, *J. Geophys. Res.*, *112*, D20113, doi:10.1029/2007JD008861.

Solomon, S., K. H. Rosenlof, R. W. Portmann, J. S. Daniel, S. M. Davis, F. J. Sanford, and G.-K. Plattner (2010), Contributions of stratospheric water vapor to decadal changes in the rate of global warming, *Science*, *327*, 1219–1223.

Vömel, H., S. J. Oltmans, D. J. Hofmann, T. Deshler, and J. M. Rosen (1995), The evolution of the dehydration in the antarctic stratospheric vortex, *J. Geophys. Res.*, *100*(D7), 13,919–13,926, doi:10.1029/95JD01000.

Wang, J. S., D. J. Seidel, and M. Free (2012), How well do we know recent climate trends at the tropical tropopause?, *J. Geophys. Res.*, *117*, D09118, doi:10.1029/2012JD017444.

World Meteorological Organization (1957), Meteorology—A three-dimensional science, *WMO Bull*, *6*, 134–138.